

1N-71
013271

Progress Report
on

NASA GRANT NAG 1-1776

JET AEROACOUSTICS: NOISE GENERATION
MECHANISM AND PREDICTION

Period covered by this report
January 1, 1998 to December 31, 1998

Principal Investigator

Dr. Christopher Tam
Department of Mathematics
Florida State University
Tallahassee, FL 32306-4510

NASA Technical Officer for this grant

John S. Preisser
Mail Stop 461
NASA Langley Research Center
Hampton, VA 23681-0001

JET AEROACOUSTICS: NOISE GENERATION MECHANISM AND PREDICTION Progress Report

This report covers the third year research effort of the project. The research work focussed on the fine scale mixing noise of both subsonic and supersonic jets and the effects of nozzle geometry and tabs on subsonic jet noise. Technical results of the research effort are reported in the following publications.

1. Tam, C.K.W. and Auriault, L. "Jet mixing noise from fine scale turbulence", AIAA Paper 98-2354, to appear in the AIAA J. Feb. 1999.
2. Tam, C.K.W. and Zaman, K.B.M., "Subsonic jet noise from non-axisymmetric and tabbed nozzles", AIAA Paper 99-0077, 1999.

(Copies of the above are attached to the end of this report.

In publication 1, a new semi-empirical theory of jet mixing noise from fine scale turbulence is developed. By an analogy to gas kinetic theory, it is shown that the source of noise is related to the time fluctuations of the turbulence kinetic theory. On starting with the Reynolds Averaged Navier-Stokes equations, a formula for the radiated noise is derived. An empirical model of the space-time correlation function of the turbulence kinetic energy is adopted. The form of the model is in good agreement with the space-time two-point velocity correlation function measured by Davies and coworkers. The parameters of the correlation are related to the parameters of the k - ϵ turbulence model. Thus the theory is self-contained. Extensive comparisons between the computed noise spectrum of the theory and experimental measured have been carried out. The parameters include jet Mach number from 0.3 to 2.0 and temperature ratio from 1.0 to 4.8. Excellent agreements are found in the spectrum shape, noise intensity and directivity. It is envisaged that the theory would supercede all semi-empirical and totally empirical jet noise prediction methods in current use.

Publication 2 uses the two similarity spectra discovered by Tam, Golebiowski and Seiner to demonstrate that the jet noise fields from circular, elliptic or rectangular nozzles are nearly identical. Nozzle shape modification is not an effective way to suppress jet noise. The effects of inserting tabs into a subsonic jet is also investigated. A jetlets model is developed to correlate the noise from a jet with N tabs to that of a single jet. The jetlets model predicts that the noise spectrum is shifted to a higher frequency by a factor of $N^{1/2}$. This result is in excellent agreement with experiments. This theory is the only theory on the noise of jets from tabbed nozzles in the literature.

AIAA Paper 98-2354

Jet Mixing Noise from Fine Scale Turbulence

Christopher K. W. Tam and Laurent Auriault
Department of Mathematics
Florida State University
Tallahassee, FL 32306-4510

Paper to be presented at the 4th AIAA/CEAS Aeroacoustics
Conference, Toulouse, France, June 2-4, 1998.

JET MIXING NOISE FROM FINE SCALE TURBULENCE[†]

Christopher K.W. Tam* and Laurent Auriault**

Florida State University
Tallahassee, FL 32306-4510

Abstract

It is known that turbulent mixing noise from high-speed jets consists of two components. They are the noise from large turbulent structures in the form of Mach wave radiation and the less directional fine scale turbulence noise. The Mach wave radiation dominates in the downstream direction. The fine scale turbulence noise dominates in the sideline and upstream directions. In this paper, a semi-empirical theory is developed for the prediction of the spectrum, intensity and directivity of the fine scale turbulence noise. The prediction method is self-contained. The turbulence information is supplied by the $k - \epsilon$ turbulence model. The theory contains three empirical constants beyond those of the $k - \epsilon$ model. These constants are determined by best fit of the calculated noise spectra to experimental measurements. Extensive comparisons between calculated and measured noise spectra over a wide range of directions of radiation, jet velocities and temperatures have been carried out. Excellent agreements are found. It is believed that the present theory offers significant improvements over current empirical or semi-empirical jet noise prediction methods in use. There is no first principle jet noise theory at the present time.

1. Introduction

Since the pioneering work of Lighthill^{1,2}, there have been numerous attempts to develop a jet noise prediction theory. In the literature, one finds many proposed theories and semi-empirical theories. The main difficulty in predicting jet noise is our lack of understanding of the turbulence in jet flows. This is true even today. However, many of the fundamental physics of jet flows that affect the propagation and radiation of jet noise were recognized very early. They have been incorporated into some of the theories. These effects include mean flow refraction^{3,4} and source motion⁵. An excellent review on jet noise

theories up to the late 1980's can be found in Ref. [6]. Ref. [7] to [9] provide reviews on the same subject. However, they include some of the more recent works and the emphasis and perspectives are quite different.

Recently, Tam, Golebiowski and Seiner¹⁰ suggested that, because there is no intrinsic characteristic length and time scales in the mixing layer of a high Reynolds number jet (up to the end of the core region), not only the mean flow and the turbulence statistics must exhibit self-similarity, the same must be true for the radiated noise. By examining the entire data bank (1900 spectra in all) of the Jet Noise Laboratory of the NASA Langley Research Center, they found that turbulent mixing noise of high-speed jets consisted of two distinct components (see also Ref. [9]). Each component exhibits self-similarity of its own. One component radiates principally in the downstream direction. This is consistent with Mach wave radiation from the large turbulence structures/instability waves of the jet flow¹¹⁻¹³. The other component that has a relatively uniform directivity is dominant in the sideline and upstream directions. These characteristics suggest that it is the noise from the fine scale turbulence of the jet flow. Tam *et al.*¹⁰ succeeded in identifying two similarity spectra from the data. They demonstrated that one of the spectra they found fitted the noise from the large turbulence structures and the other the noise from the fine scale turbulence regardless of the jet velocity, temperature and direction of radiation. More recently, Tam¹⁴ showed that even the noise spectra of non-axisymmetric jets including jets from rectangular, elliptic, plug and suppressor nozzles fitted the same two empirically found similarity spectra. This indicates that the noise sources of these jets are similar to those of the circular jet. Their noise is also made up of two components.

The primary objective of this work is to develop a semi-empirical theory for the prediction of the fine scale turbulence noise from high-speed jets. The present theory is self-contained. The turbulence information of the jet flow needed for noise prediction are supplied by the $k - \epsilon$ turbulence model. Since the $k - \epsilon$ model is a semi-empirical model, the present theory is also semi-empirical. As will become clear later, the noise prediction formula developed here

[†] Copyright ©1998 by C.K.W. Tam. Published by the Confederation of European Aerospace Societies with permission.

* Distinguished Research Professor, Department of Mathematics. Associate Fellow AIAA.

** Graduate student, Department of Mathematics.

contains three empirical constants. These constants are determined by best fit to the noise data. Once the constants are decided, the formula can provide accurate noise spectrum and directivity predictions over the jet velocity ratio range of $\frac{u_j}{a_\infty} = 0.4$ to 3.0 (u_j and a_∞ are the fully expanded jet velocity and ambient sound speed) and temperature ratio range of $\frac{T_r}{T_\infty} = 1.0$ to 5.0 (T_r and T_∞ are the jet reservoir and ambient temperature). This parametric range brackets all known jet noise experiments and commercial jet engine operating conditions.

The use of the $k-\varepsilon$ turbulence model to predict jet noise is not new. Khavaran, Krejsa and Kim^{15,16}, Bailly and coworkers¹⁷⁻²⁰ employed the $k-\varepsilon$ model to provide turbulence statistics to their chosen version of the acoustic analogy theory for supersonic jet noise prediction. Khavaran *et al.* tuned their empirical constants to fit the measured jet noise data at Mach 1.4. However, even at this Mach number, the calculated spectra do not fit the measured data well at 90 degrees and in the forward direction for which the fine scale turbulence noise dominates. Bailly and coworkers were more interested in using their model to calculate Mach wave radiation from supersonic jets. There is fair agreement between their computed and measured directivity data but the calculated spectral distributions do not match well with experiments.

To develop a fine scale turbulence noise theory requires many steps. We will first turn to the question of how fine scale turbulence in a jet generates sound. For this purpose, we will use the gas kinetic theory analogy. The use of gas kinetic theory to elucidate ideas in turbulence is well established²¹. Consider the motion of gas molecules in a moving frame fixed to the mean velocity $\bar{\mathbf{v}}$ as shown in figure 1. Suppose m is the mass of a molecule, n is the number density. Due to the random motion of the gas molecules, the gas exerts a pressure, p , on its surroundings. It is a simple matter to show, following standard kinetic theory of gases^{22,23}, that p is given by,

$$p = \frac{1}{3}mn\langle \mathbf{v} \cdot \mathbf{v} \rangle = \frac{1}{3}\rho\langle v^2 \rangle \quad (1)$$

where \mathbf{v} is the random molecular velocity. ρ is the density of the gas and $\langle \rangle$ is the ensemble average.

Now we will regard fine scale turbulence as small blobs of fluid moving randomly as shown in figure 2. Again, let \mathbf{v} be the random velocity of the fine scale turbulence measured in the mean flow moving frame. By analogy to the gas molecules of figure 1, the fine scale turbulence effectively exerts a pressure, p_{turb} ,

on its surroundings. This pressure, following (1), is equal to

$$p_{\text{turb}} = q_s \equiv \frac{1}{3}\rho\langle v^2 \rangle = \frac{2}{3}\rho k_s, \quad (2)$$

where $k_s = \frac{1}{2}\langle v^2 \rangle$ is the kinetic energy of the fine scale turbulence per unit mass. The pressure given by (2) is a macroscopic quantity valid for length scale larger than the size of an individual blob of turbulent fluid. This pressure must be balanced by pressure and momentum flux of the surrounding fluid. If this pressure fluctuates in time, it will inevitably give rise to compressions and rarefactions in the fluid medium. This results in acoustic disturbances. Following this reasoning, one would expect the source of fine scale turbulence noise to be equal to the time rate of change of p_{turb} or q_s in the moving frame of the fluid. In other words, $\frac{Dq_s}{Dt}$, the convective derivative of q_s , is the noise source term in a turbulent flow.

In section 2, the equations governing the generation and propagation of acoustic disturbances in a jet flow (generated by fine scale turbulence) are formally derived. Here we will begin with the Reynolds Averaged Navier-Stokes equations (RANS). The relationship between the radiated sound field and the source of fine scale turbulence noise will be established. In section 3, a semi-empirical model of the noise source space-time correlation function is developed. The parameters of the correlation function are then related to the length and time scales of the $k-\varepsilon$ turbulence model. By means of this source correlation function, a formula for the spectrum of the radiated noise is derived. Extensive comparisons between the calculated results of this formula and experimental measurements have been carried out. A sample of these comparisons are reported in section 4. Good agreements are found over both subsonic and supersonic Mach number. Temperature dependence over a wide range of jet to ambient temperature ratios is also correctly predicted.

2. Formulation

Consider the flow of a turbulent compressible jet. A convenient way to account for the effect of compressibility is to use Favre average variables²⁴. For the present purpose, we may regard the average as a volume average²⁵ with a sharp Fourier cutoff filter; the volume being smaller than the large turbulence structures of the jet flow but larger than the fine scale turbulence. We will decompose a flow variable into two parts,

$$f = \tilde{f} + f'' \quad (3)$$

where \tilde{f} and f'' are the Favre average and Favre fluctuating components. On starting from the equations of motion, it is straightforward to derive the familiar Reynolds averaged Navier-Stokes equations (RANS); e.g., see Ref. [26].

$$\begin{aligned} \bar{\rho} \left(\frac{\partial \tilde{u}_i}{\partial t} + \tilde{u}_j \frac{\partial \tilde{u}_i}{\partial x_j} \right) \\ = - \frac{\partial \bar{p}}{\partial x_i} + \frac{\partial}{\partial x_j} \left(-\overline{\rho u_i'' u_j''} + \bar{\tau}_{ij} \right) \end{aligned} \quad (4)$$

where an overbar denotes a Reynolds averaged quantity. The terms $\bar{\tau}_{ij}$ and $-\overline{\rho u_i'' u_j''}$ on the right side of (4) are the viscous and Reynolds stresses, respectively. On following the generally accepted RANS approach, we will adopt the Boussinesq eddy viscosity model for the Reynolds stresses; i.e.,

$$-\overline{\rho u_i'' u_j''} = 2\mu_t \left(S_{ij} - \frac{1}{3} \Delta \delta_{ij} \right) - \frac{2}{3} \bar{\rho} k_s \delta_{ij} \quad (5)$$

where μ_t is the eddy viscosity and

$$S_{ij} = \frac{1}{2} \left(\frac{\partial \tilde{u}_i}{\partial x_j} + \frac{\partial \tilde{u}_j}{\partial x_i} \right), \quad \Delta = \frac{\partial \tilde{u}_k}{\partial x_k} \quad (6)$$

$$-\overline{\rho u_i'' u_i''} = 2\bar{\rho} k_s. \quad (7)$$

Of importance is that k_s as defined by (7) is the kinetic energy of the fine scale turbulence per unit mass.

As discussed in the previous section, k_s in (5) effectively represents a pressure field exerted by the fine scale turbulence on the surrounding fluid. The time fluctuation of this pressure field causes compressions and rarefactions in the fluid medium. In this way, sound is generated by the small scale turbulence. Inside the jet flow, the acoustic field is a very small part of the unsteady fluctuations. It is sufficient to consider the acoustic field generated by the time dependent part of k_s , denoted by \hat{k}_s , to be given by the linearized form of equations (4) and (5). The linearization is to be performed over the mean flow of the jet. In addition, both molecular and eddy viscosity terms will be ignored as they will have only a relatively small effect on the acoustic disturbances. The linearized form of (4) with only \hat{k}_s terms retained on the right side, after applying the locally parallel mean flow approximation, is

$$\bar{\rho} \left[\frac{\partial u_i}{\partial t} + \bar{u}_j \frac{\partial u_i}{\partial x_j} + u_i \frac{\partial \bar{u}_j}{\partial x_j} \right] + \frac{\partial p}{\partial x_i} = - \frac{\partial q_s}{\partial x_i} \quad (8)$$

where

$$q_s = \frac{2}{3} \bar{\rho} \hat{k}_s \quad (9)$$

is the unsteady pressure exerted by the fine scale turbulence. In (8), \bar{u}_i and $\bar{\rho}$ are the mean velocity and density of the jet and u_i , p are the acoustic field variables associated with \hat{k}_s . We will now supplement equation (8) with the linearized continuity and energy equation (ignoring viscous and thermal dissipations) to form a closed system of equations for the acoustic field. With respect to a cylindrical coordinate system (r, ϕ, x) centered at the nozzle exit (with the x -axis coinciding with the jet axis), the full set of governing equations are,

$$\bar{\rho} \left[\frac{\partial u}{\partial t} + \bar{u} \frac{\partial u}{\partial x} + v \frac{d\bar{u}}{dr} \right] + \frac{\partial p}{\partial x} = - \frac{\partial q_s}{\partial x} \quad (10a)$$

$$\bar{\rho} \left[\frac{\partial v}{\partial t} + \bar{u} \frac{\partial v}{\partial x} \right] + \frac{\partial p}{\partial r} = - \frac{\partial q_s}{\partial r} \quad (10b)$$

$$\bar{\rho} \left[\frac{\partial w}{\partial t} + \bar{u} \frac{\partial w}{\partial x} \right] + \frac{1}{r} \frac{\partial p}{\partial \phi} = - \frac{1}{r} \frac{\partial q_s}{\partial \phi} \quad (10c)$$

$$\begin{aligned} \frac{\partial p}{\partial t} + \bar{u} \frac{\partial p}{\partial x} + \gamma \bar{p} \left[\frac{1}{r} \frac{\partial (vr)}{\partial r} + \frac{1}{r} \frac{\partial w}{\partial \phi} + \frac{\partial u}{\partial x} \right] \\ = 0. \end{aligned} \quad (10d)$$

In these equations (u, v, w) are the velocity components in the (x, r, ϕ) directions. Also, in accordance of the locally parallel flow approximation, $\bar{\rho}$, \bar{u} are regarded as functions of r alone and $\bar{p} = p_\infty$ is constant.

2.1. The Acoustic Field

Equations (10a) to (10d), except for the noise source terms on the right, are identical to the Lilley's equation^{4,6}. As is well known, the Lilley's approach was designed to account for the mean flow refraction effect. This effect is especially significant for the high frequency part of the noise spectrum. This is confirmed in the numerical results reported in section 4.

A formal solution of (10) directly relating the radiated acoustic pressure field to the fine scale turbulence intensity q_s can be found by using the space-time Green's function of these equations. Since q_s appears on the right side of equations (10a), (10b) and (10c), three Green's functions are necessary. Let (u_n, v_n, w_n, p_n) with $n = 1, 2$ and 3 be the Green's functions corresponding to a source on the right side of equations (10a), (10b) or (10c), respectively. These Green's functions satisfy the following nonhomogeneous equations.

$$\begin{aligned} \bar{\rho} \left[\frac{\partial u_n}{\partial t} + \bar{u} \frac{\partial u_n}{\partial x} + v_n \frac{d\bar{u}}{dr} \right] + \frac{\partial p_n}{\partial x} \\ = \delta(\mathbf{x} - \mathbf{x}_1) \delta(t - t_1) \delta_{n1} \end{aligned} \quad (11)$$

$$\bar{p} \left[\frac{\partial v_n}{\partial t} + \bar{u} \frac{\partial v_n}{\partial x} \right] + \frac{\partial p_n}{\partial r} = \delta(\mathbf{x} - \mathbf{x}_1) \delta(t - t_1) \delta_{n2} \quad (12)$$

$$\bar{p} \left[\frac{\partial w_n}{\partial t} + \bar{u} \frac{\partial w_n}{\partial x} \right] + \frac{1}{r} \frac{\partial p_n}{\partial \phi} = \delta(\mathbf{x} - \mathbf{x}_1) \delta(t - t_1) \delta_{n3} \quad (13)$$

$$\frac{\partial p_n}{\partial t} + \bar{u} \frac{\partial p_n}{\partial x} + \gamma \bar{p} \left[\frac{1}{r} \frac{\partial(v_n r)}{\partial r} + \frac{1}{r} \frac{\partial w_n}{\partial \phi} + \frac{\partial u_n}{\partial x} \right] = 0 \quad (14)$$

where $n = 1, 2, 3$. Here $\delta(\cdot)$ is the Dirac delta function and δ_{nm} is the Kronecker delta. The Green's functions depend on four variables. They are the field or observer coordinates, \mathbf{x} , the source coordinates, \mathbf{x}_1 , the field or observation time, t , and the source time, t_1 . To avoid confusion, whenever it is necessary to display the arguments of the Green's function, they will always be in exactly this order; e.g., $p_n(\mathbf{x}, \mathbf{x}_1, t, t_1)$.

The space-time Green's function is related to the time harmonic Green's function ($\hat{u}_n, \hat{v}_n, \hat{w}_n, \hat{p}_n$) by the Fourier inverse transform. For example, we have

$$p_n(\mathbf{x}, \mathbf{x}_1, t, t_1) = \int_{-\infty}^{\infty} \hat{p}_n(\mathbf{x}, \mathbf{x}_1, \omega) e^{-i\omega(t-t_1)} d\omega \quad (15)$$

The equations governing the time harmonic Green's functions are simply the Fourier transforms of (11) to (14). Recently the present authors²⁷ have shown that there is great computational advantage to use the adjoint time harmonic Green's function instead of the time harmonic Green's functions. On following the work of Ref. [27], it is easy to find that the adjoint time harmonic Green's function (u_a, v_a, w_a, p_a) (subscript a indicates the adjoint) satisfies the following equations.

$$-\bar{p} \left[i\omega u_a + \bar{u} \frac{\partial u_a}{\partial x} \right] - \gamma \bar{p} \frac{\partial p_a}{\partial x} = 0 \quad (16)$$

$$-\bar{p} \left[i\omega v_a + \bar{u} \frac{\partial v_a}{\partial x} - \frac{d\bar{u}}{dr} u_a \right] - \gamma \bar{p} \frac{\partial p_a}{\partial r} = 0 \quad (17)$$

$$-\bar{p} \left[i\omega w_a + \bar{u} \frac{\partial w_a}{\partial x} \right] - \frac{\gamma \bar{p}}{r} \frac{\partial p_a}{\partial \phi} = 0. \quad (18)$$

$$-i\omega p_a - \bar{u} \frac{\partial p_a}{\partial x} - \left[\frac{1}{r} \frac{\partial(v_a r)}{\partial r} + \frac{1}{r} \frac{\partial w_a}{\partial \phi} + \frac{\partial u_a}{\partial x} \right] = \frac{1}{2\pi} \delta(\mathbf{x} - \mathbf{x}_1) \quad (19)$$

It is straightforward to show that the pressure fields of the three original time harmonic Green's

functions are related to the adjoint Green's function by²⁷,

$$\begin{aligned} \hat{p}_1(\mathbf{x}, \mathbf{x}_1, \omega) &= u_a(\mathbf{x}_1, \mathbf{x}, \omega) \\ \hat{p}_2(\mathbf{x}, \mathbf{x}_1, \omega) &= v_a(\mathbf{x}_1, \mathbf{x}, \omega) \\ \hat{p}_3(\mathbf{x}, \mathbf{x}_1, \omega) &= w_a(\mathbf{x}_1, \mathbf{x}, \omega). \end{aligned} \quad (20)$$

It is worthwhile to point out that the arguments on the two sides of equation (20) satisfy the reciprocity relation. That is, the source point and the field point of the adjoint are interchanged. It is clear from (20) that there is another important advantage in using the adjoint Green's function. If one is interested in the far acoustic field, namely, the pressure field, it is only necessary to solve the adjoint equations (16) to (19) once to obtain (u_a, v_a, w_a). On the other hand, to find \hat{p}_1, \hat{p}_2 and \hat{p}_3 directly one has to solve the original time harmonic Green's function equations three times.

By means of the adjoint Green's function, the pressure field generated by the source terms on the right side of (10a) to (10d) is formally given by,

$$\begin{aligned} p(\mathbf{x}, t) &= - \iiint_{-\infty}^{\infty} \iiint_{-\infty}^{\infty} \iiint_{-\infty}^{\infty} \left[u_a(\mathbf{x}_1, \mathbf{x}, \omega) \frac{\partial q_s(\mathbf{x}_1, t_1)}{\partial x_1} \right. \\ &\quad + v_a(\mathbf{x}_1, \mathbf{x}, \omega) \frac{\partial q_s(\mathbf{x}_1, t_1)}{\partial r_1} \\ &\quad \left. + \frac{w_a(\mathbf{x}_1, \mathbf{x}, \omega)}{r} \frac{\partial q_s(\mathbf{x}_1, t_1)}{\partial \phi} \right] \\ &\quad \cdot e^{-i\omega(t-t_1)} d\omega dt_1 d\mathbf{x}_1. \end{aligned} \quad (21)$$

Let $\nabla_1 \equiv (\frac{\partial}{\partial x_1} \mathbf{e}_x + \frac{\partial}{\partial y_1} \mathbf{e}_y + \frac{\partial}{\partial z_1} \mathbf{e}_z)$ be the gradient with respect to the \mathbf{x}_1 coordinates. (21) may be rewritten in the form,

$$\begin{aligned} p(\mathbf{x}, t) &= - \iiint_{-\infty}^{\infty} \iiint_{-\infty}^{\infty} \iiint_{-\infty}^{\infty} [\nabla_1 \cdot (\mathbf{v}_a(\mathbf{x}_1, \mathbf{x}, \omega) q_s(\mathbf{x}_1, t_1)) \\ &\quad - q_s(\mathbf{x}_1, t_1) \nabla_1 \cdot \mathbf{v}_a(\mathbf{x}_1, \mathbf{x}, \omega)] \\ &\quad \cdot e^{-i\omega(t-t_1)} d\omega dt_1 d\mathbf{x}_1 \end{aligned} \quad (22)$$

where $\mathbf{v}_a = (u_a, v_a, w_a)$. This formula can be simplified in two ways. First, we can apply the divergence theorem to the first term of the integrand. This converts the volume integral $d\mathbf{x}_1$ to a surface integral outside the jet flow. But q_s is zero outside the jet. Thus, there is no contribution from the first term. Now for $\mathbf{v}_a(\mathbf{x}_1, \mathbf{x}, \omega)$, the source is outside the jet flow if \mathbf{x} is in the far field. Thus by making use of (19),

(22) becomes,

$$\begin{aligned}
p(\mathbf{x}, t) &= - \iiint\limits_{\mathbf{x} \text{ outside the jet}} \iiint\limits_{-\infty}^{\infty} q_s(\mathbf{x}_1, t_1) \left[\left(i\omega + \bar{u} \frac{\partial}{\partial x_1} \right) \right. \\
&\quad \left. \cdot p_a e^{-i\omega(t-t_1)} d\omega \right] dt_1 d\mathbf{x}_1 \\
&= - \iiint\limits_{\mathbf{x} \text{ outside the jet}} \iiint\limits_{-\infty}^{\infty} q_s(\mathbf{x}_1, t_1) \left[\left(\frac{\partial}{\partial t_1} + \bar{u} \frac{\partial}{\partial x_1} \right) \right. \\
&\quad \left. \cdot p_a e^{-i\omega(t-t_1)} d\omega \right] dt_1 d\mathbf{x}_1.
\end{aligned}$$

Finally, by simple integration by parts, we find the desirable formula for $p(\mathbf{x}, t)$,

$$\begin{aligned}
p(\mathbf{x}, t) &= \iiint\limits_{\mathbf{x} \text{ outside the jet}} \iiint\limits_{-\infty}^{\infty} \left[\int\limits_{-\infty}^{\infty} p_a(\mathbf{x}_1, \mathbf{x}, \omega) \right. \\
&\quad \left. \cdot e^{-i\omega(t-t_1)} d\omega \right] \frac{Dq_s(\mathbf{x}_1, t_1)}{Dt_1} dt_1 d\mathbf{x}_1
\end{aligned} \quad (23)$$

where $\frac{D}{Dt_1} = \frac{\partial}{\partial t_1} + \bar{u} \frac{\partial}{\partial x_1}$ is the convective derivative following the mean flow.

Equation (23) is the main result of this section. Obviously, it is open to the interpretation that noise from fine scale turbulence is generated by the time rate of change of the turbulence kinetic energy or pressure in the moving frame following the convection of the fine scale turbulence by the mean flow. The term inside the square bracket is the adjoint Green's function with the source located at \mathbf{x} and the field point at \mathbf{x}_1 according to the reciprocity relation.

2.2. The Spectral Density of the Radiated Sound

By means of (23), the autocorrelation function for a point in the acoustic far field may be formed; i.e.,

$$\begin{aligned}
\langle p(\mathbf{x}, t) p(\mathbf{x}, t + \tau) \rangle &= \iiint\limits_{-\infty}^{\infty} \iiint\limits_{-\infty}^{\infty} p_a(\mathbf{x}_1, \mathbf{x}, \omega_1) \\
&\quad \cdot p_a(\mathbf{x}_2, \mathbf{x}, \omega_2) \left\langle \frac{Dq_s(\mathbf{x}_1, t_1)}{Dt_1} \frac{Dq_s(\mathbf{x}_2, t_2)}{Dt_2} \right\rangle \\
&\quad \cdot e^{-i\omega_1(t-t_1) - i\omega_2(t-t_2) - i\omega_2\tau} d\omega_1 d\omega_2 dt_1 dt_2 d\mathbf{x}_1 d\mathbf{x}_2.
\end{aligned} \quad (24)$$

In (24), $\langle \rangle$ is the ensemble average.

The spectral density of the radiated sound, $S(\mathbf{x}, \omega)$ is the Fourier transform of the autocorrelation function or

$$S(\mathbf{x}, \omega) = \frac{1}{2\pi} \int\limits_{-\infty}^{\infty} \langle p(\mathbf{x}, t) p(\mathbf{x}, t + \tau) \rangle e^{i\omega\tau} d\tau. \quad (25)$$

By using $\int\limits_{-\infty}^{\infty} \exp[i(\omega - \omega_2)\tau] d\tau = 2\pi\delta(\omega - \omega_2)$, it is straightforward to derive from (24), the following formula for $S(\mathbf{x}, \omega)$.

$$\begin{aligned}
S(\mathbf{x}, \omega) &= \iiint\limits_{-\infty}^{\infty} \iiint\limits_{-\infty}^{\infty} p_a(\mathbf{x}_1, \mathbf{x}, \omega_1) p_a(\mathbf{x}_2, \mathbf{x}, \omega_2) \\
&\quad \cdot \left\langle \frac{Dq_s(\mathbf{x}_1, t_1)}{Dt_1} \frac{Dq_s(\mathbf{x}_2, t_2)}{Dt_2} \right\rangle \\
&\quad \cdot e^{-i(\omega_1 + \omega_2)t + i\omega_1 t_1 + i\omega_2 t_2} \\
&\quad \cdot \delta(\omega - \omega_2) d\omega_1 d\omega_2 dt_1 dt_2 d\mathbf{x}_1 d\mathbf{x}_2.
\end{aligned} \quad (26)$$

3. Model Space-Time Correlation Function

To proceed further, we need a mathematical representation of the noise source space-time correlation function $\left\langle \frac{Dq_s(\mathbf{x}_1, t_1)}{Dt_1} \frac{Dq_s(\mathbf{x}_2, t_2)}{Dt_2} \right\rangle$. This correlation function has never been measured before. However, two-point space-time correlation of the fluctuating axial velocity component in jets has been measured and studied by Davies, Fisher and Barrett²⁸ and Chu²⁹. We believe that the mathematical form of $\left\langle \frac{Dq_s}{Dt_1} \frac{Dq_s}{Dt_2} \right\rangle$ should be similar to that of the measured two-point space-time correlation function of the axial velocity component. Here we propose to adopt a model space-time correlation function characterized by three parameters. We will show that with an appropriate choice of the parameters, the model function fits the measured function of Davies *et al.* (see figure 3) well.

Let $\xi = x_1 - x_2$, $\eta = y_1 - y_2$, $\zeta = z_1 - z_2$, $\tau = t_1 - t_2$. We will consider the following model function

$$\begin{aligned}
\left\langle \frac{Dq_s(\mathbf{x}_1, t_1)}{Dt_1} \frac{Dq_s(\mathbf{x}_2, t_2)}{Dt_2} \right\rangle &= \frac{\hat{q}_s^2}{c^2 \tau_s^2} \\
&\quad \cdot e^{-\frac{\ell_s}{\bar{u} \tau_s} - \frac{\ln 2}{\tau_s^2} [(\xi - \bar{u} \tau)^2 + \eta^2 + \zeta^2]}
\end{aligned} \quad (27)$$

In (27) \bar{u} is the mean flow velocity or the transport velocity of the fine scale turbulence. The three parameters of the model are ℓ_s , τ_s and \hat{q}_s^2 . ℓ_s is the characteristic size of the fine scale turbulence in the moving frame of the mean flow. τ_s is the characteristic decay time. $\bar{u} \tau_s$ is the decay distance. In the limit $\xi, \eta, \zeta, \tau \rightarrow 0$, (27) becomes

$$\left\langle \left(\frac{Dq_s(\mathbf{x}, t)}{Dt} \right)^2 \right\rangle = \frac{\hat{q}_s^2}{c^2 \tau_s^2}. \quad (28)$$

Thus \hat{q}_s is a measure of the RMS value of the fluctuating kinetic energy of the fine scale turbulence and

$c\tau$, represents a typical time scale of the fluctuation. The coefficient c is expected to be less than 1.0. This indicates that the fluctuating time is shorter than the turbulence decay time.

Figure 3 shows a plot of the correlation function (27) with $\ell_s = 0.1758$ inches, $\tau_s = 447.4 \mu$ sec. and $\bar{u} = 3.515 \times 10^{-3}$ inch/ μ sec. As can be seen, the model function is in reasonably good agreement with the measurements of Davies *et al.*²⁸. This result assures us that the model space-time correlation function does have the right functional characteristics. We will use this model correlation function throughout this work.

Model correlation function (27) has three parameters, namely, ℓ_s , τ_s and \hat{q}_s . They are the characteristic parameters of the fine scale turbulence of the jet flow. Here we propose to obtain the values of these parameters through the $k - \epsilon$ turbulence model.

It is generally known that the standard $k - \epsilon$ turbulence model does poorly in predicting the mean flow of jets³⁰. Thies and Tam³¹ recognized the problem of applying the standard $k - \epsilon$ model to jet flows. They proposed to modify the $k - \epsilon$ model coefficients and showed convincingly by comparison with a large set of jet flow data over the jet Mach number range of 0.4 to 2.0 and temperature ratio of 1.0 (cold jet) to 4.0 that their modified $k - \epsilon$ model is reliable and accurate. In this work, the modified $k - \epsilon$ model of Ref. [31] is used.

The $k - \epsilon$ model provides only two pieces of information about the turbulence of the jet flow. They are k , the averaged turbulence kinetic energy, and ϵ , the dissipation rate. But with k and ϵ known, it is possible to form a length ℓ , characterizing the size of the small scale turbulence and a decay time, τ , of the turbulence as follows,

$$\ell = \frac{k^{\frac{3}{2}}}{\epsilon}, \quad \tau = \frac{k}{\epsilon}. \quad (29)$$

The parameters ℓ and τ of (29) are directly relevant to the parameters ℓ_s and τ_s of model two-point space-time correlation function (27). To establish their relationship, we performed a $k - \epsilon$ model calculation for the jet flow of the Davies *et al.* experiment. At the location of the measured correlation function shown in figure 3, the value of ℓ and τ obtained were very close to 0.176 inches and 447 μ sec., respectively. These are the values of ℓ_s and τ_s used to match correlation function (27) to the measurements. We, therefore, believe that ℓ_s and τ_s of our model correlation function is directly related to ℓ and τ of the $k - \epsilon$ model. However, the $k - \epsilon$

model includes contributions from the large turbulence structures whereas ℓ_s and τ_s are those of the fine scale turbulence alone. On accounting for this difference, we propose to let,

$$\ell_s = c_\ell \ell = c_\ell \frac{k^{\frac{3}{2}}}{\epsilon}, \quad \tau_s = c_\tau \tau = c_\tau \frac{k}{\epsilon} \quad (30)$$

where c_ℓ and c_τ ($c_\ell, c_\tau < 1.0$) are constants to be determined empirically.

In the above, we have noted that \hat{q}_s is a measure of the intensity of the fluctuation of the kinetic energy of the fine scale turbulence. We, therefore, expect it to be proportional to q . ($q = \frac{2}{3} \bar{p} k$.) We will let

$$\frac{\hat{q}_s^2}{c^2} = A^2 q^2 \quad (31)$$

where A is the third empirical constant.

With (30) and (31), the two-point space-time correlation function (27) is known save for the three constants c_ℓ , c_τ and A . These constants are to be determined by best fit of the calculated noise spectra to experimental measurements.

4. A Formula for the Noise Spectrum

On substitution of (27) into (26), the noise spectrum in the far field is given by

$$\begin{aligned} S(\mathbf{x}, \omega) = & \iiint_{-\infty}^{\infty} \iiint_{-\infty}^{\infty} p_a(\mathbf{x}_1, \mathbf{x}, \omega_1) p_a(\mathbf{x}_2, \mathbf{x}, \omega_2) \frac{\hat{q}_s^2}{c^2 \tau_s^2} \\ & \cdot e^{-\frac{|\mathbf{x}_1 - \mathbf{x}_2|}{\bar{u}} - \frac{\ln 2}{\ell_s^2} [(x_1 - x_2 - \bar{u}(t_1 - t_2))^2 + (y_1 - y_2)^2 + (z_1 - z_2)^2]} \\ & \cdot e^{-i(\omega_1 + \omega_2)t + i\omega_1 t_1 + i\omega_2 t_2} \\ & \cdot \delta(\omega - \omega_2) dt_1 dt_2 d\omega_2 d\omega_2 d\mathbf{x}_1 d\mathbf{x}_2 \end{aligned} \quad (32)$$

We will now show that most of the above integrals can be evaluated analytically. The entire expression can be reduced to a single volume integral over the jet flow.

The first step is to integrate dt_1 . The integration can best be carried out by first making a change of variable to s where

$$s = (t_1 - t_2) - \frac{(x_1 - x_2)}{\bar{u}}$$

Next, the t_2 integration can be performed resulting in $2\pi\delta(\omega_1 + \omega_2)$. With $\delta(\omega_1 + \omega_2)$ and $\delta(\omega - \omega_2)$ in the integrand, the ω_1 and ω_2 integrals can be readily evaluated giving

$$\begin{aligned} S(\mathbf{x}, \omega) = & 2\pi \left(\frac{\pi}{\ln 2} \right)^{\frac{1}{2}} \iiint_{-\infty}^{\infty} \iiint_{-\infty}^{\infty} \frac{\hat{q}_s^2}{c^2 \tau_s^2} \frac{\ell_s}{\bar{u}} \\ & \cdot p_a(\mathbf{x}_1, \mathbf{x}, -\omega) p_a(\mathbf{x}_2, \mathbf{x}, \omega) e^{-\frac{\omega^2 \ell_s^2}{\bar{u}^2 (4 \ln 2)} - \frac{|\mathbf{x}_1 - \mathbf{x}_2|}{\bar{u}}} \\ & \cdot e^{-\frac{\ln 2}{\ell_s^2} [(y_1 - y_2)^2 + (z_1 - z_2)^2] - \frac{i\omega(x_1 - x_2)}{\bar{u}}} d\mathbf{x}_1 d\mathbf{x}_2. \end{aligned} \quad (33)$$

In (33), the integrand is nearly zero unless \mathbf{x}_1 is close to \mathbf{x}_2 . Since \mathbf{x} is in the far field, the adjoint Green's function $p_a(\mathbf{x}_1, \mathbf{x}, -\omega)$ and $p_a(\mathbf{x}_2, \mathbf{x}, -\omega)$ differ primarily by a phase factor. The phase difference can be assessed by ray acoustics. Figure 4 shows the rays from a far away point \mathbf{x} to \mathbf{x}_1 and \mathbf{x}_2 . The rays are essentially parallel except after entering the jet flow. We will now use a spherical polar coordinate system centered at the nozzle exit with the polar axis coinciding with the x -axis, or the jet axis. Let the spherical coordinates of \mathbf{x} be (R, Θ, ϕ) where Θ is the polar angle. The paths for the rays to \mathbf{x}_1 and \mathbf{x}_2 differ by a length nearly equal to $AC = (x_1 - x_2) \cos \Theta$ (see figure 4). The phase difference is equal to wavenumber times the difference in path lengths. Thus, the two adjoint Green's functions differ by a phase factor of $\exp[i\frac{\omega}{a_\infty} \cos \Theta (x_1 - x_2)]$ where a_∞ is the ambient sound speed.

We will now adopt the approximation

$$p_a(\mathbf{x}_1, \mathbf{x}, -\omega) \simeq p_a(\mathbf{x}_2, \mathbf{x}, -\omega) e^{i\frac{\omega}{a_\infty} \cos \Theta (x_1 - x_2)}. \quad (34)$$

(34) may also be obtained by invoking a locally parallel flow approximation. On substitution of (34) into (33) and on noting that $p_a(\mathbf{x}_2, \mathbf{x}, -\omega) = p_a^*(\mathbf{x}_2, \mathbf{x}, \omega)$ where $*$ indicates the complex conjugate, the integrals over \mathbf{x}_1 can be easily evaluated. This gives,

$$S(\mathbf{x}, \omega) = 4\pi \left(\frac{\pi}{\ln 2} \right)^{\frac{3}{2}} \int_{-\infty}^{\infty} \int_{-\infty}^{\infty} \frac{\hat{q}_s^2 \ell_s^3}{c^2 \tau_s} \cdot \frac{|p_a(\mathbf{x}_2, \mathbf{x}, \omega)|^2 e^{-\frac{\omega^2 \ell_s^2}{\bar{u}^2 (4 \ln 2)}}}{[1 + \omega^2 \tau_s^2 (1 - \frac{\bar{u}}{a_\infty} \cos \Theta)^2]} d\mathbf{x}_2. \quad (35)$$

The spectral density $S(\mathbf{x}, \omega)$ has the dimensions of (pressure)²time. On converting to dB per Strouhal number ($\frac{f D_j}{u_j}$; u_j and D_j are the fully expanded jet velocity and diameter) the spectral density of the sound pressure field at (R, Θ, ϕ) is,

$$S \left(R, \Theta, \phi; \frac{f D_j}{u_j} \right) = 10 \log \left[\frac{4\pi S(\mathbf{x}, \omega)}{p_{\text{ref}}^2 \frac{D_j}{u_j}} \right] \quad (36)$$

where p_{ref} is the reference pressure of the decibel scale.

5. Comparisons with Experiments

Before we compare the numerical results of formulas (36) and (35) with experimental measurements, it is believed worthwhile to describe briefly

how the various quantities and integrals of these formulas are determined and evaluated. Essentially the computations are carried out in three steps. First, with a prescribed jet operating condition, the mean flow and the values of k and ε are calculated following Ref. [31]. Once k and ε are found, ℓ_s , τ_s and $\frac{\bar{u}}{c}$ are determined by (30) and (31). The second step is to make use of the calculated mean flow to find the adjoint Green's function as in Ref. [27]. Finally, the volume integral is evaluated by dividing the jet axially into slices of 0.5 diameter. Azimuthally, the adjoint Green's function is expressed in Fourier modes. They are summed over. In the radial direction, a very fine mesh is used in the volume integration.

We will compare formula (36) with four sets of data. They are the data of the Jet Noise Laboratory of the NASA Langley Research Center measured by Seiner¹⁰ and his coworkers, the Norum & Brown³², Tanna *et al.*³³ and Ahuja³⁴ data. The NASA Langley data are from supersonic jets at temperature ratio of 1.0 to 4.9. The Norum & Brown data include both subsonic and supersonic cold jets. The Tanna *et al.* data are from subsonic and supersonic jets. Only hot jet data at supersonic Mach number are considered of good quality to be included for comparison. The Ahuja data are all at subsonic Mach number at room temperature. There is overall consistency among the four sets of data. However, for hot jets at supersonic speed, the NASA data is approximately 1 to 2 dB higher than the Tanna *et al.* measurements. Generally speaking, we believe that there is an uncertainty in the data of the order of 1 to 2 dB.

Before formulas (35) and (36) can be used, the three empirical constants c_ℓ , c_τ and A have to be determined. After some trial and error to obtain best fit to the data, the following values are selected,

$$c_\ell = 0.256, \quad c_\tau = 0.233 \quad \text{and} \quad A = 0.755. \quad (37)$$

These are the values used throughout the rest of the paper.

Figures 5a, b, c show comparisons of the calculated noise spectra and the experimental measurements of Ref. [10] and [32] at $\frac{T_r}{T_\infty} = 1.0$. The spectra are scaled to a distance of $100 D_j$. Shown in these figures are data from jets at fully expanded jet Mach number $M_j = 2.0, 1.49, 0.9, 0.7, 0.5$ and 0.3 . Figure 5a is for noise radiation at $\Theta = 60$ deg. As can be seen, there are excellent agreements between the calculated spectra and measurements except at very high frequency. At very high frequency, the measurements are less reliable as they

are close to the high frequency cut-off of the microphones. Figure 5b shows similar comparisons at $\Theta = 90$ deg. The agreements are again excellent except for the $M_j = 1.49$ case. The two broadband peaks on the high frequency side of the spectrum are broadband shock associated noise^{35,7,8}. They should be ignored in the comparison. In Ref. [10], this was noticed when comparing the spectrum of a perfectly expanded jet against that of an imperfectly expanded jet at identical operating conditions. Figure 5c shows the comparisons at $\Theta = 120$ deg. Again, there are good agreements. In the forward direction, most supersonic jet spectra, invariably, contain broadband shock noise. The difference between the calculated and measured spectra at $M_j = 2.0$ and 1.49 is mainly due to the presence of broadband shock associated noise.

Figure 6 shows the comparisons of hot jet spectra. The jet Mach number and temperature ratio are fixed at 2.0 and 1.8, respectively. The spectra in three directions are provided. There are good agreements between the calculated spectra and the experimental measurements. This is true both in the peak level and spectral shape. The slight difference for the case at $\Theta = 117$ deg. is again due to the presence of broadband shock associated noise in the forward direction.

To test whether formula (36) can predict accurately the change in noise spectrum with jet temperature, the noise data of Ref. [10] at Mach 2.0 in the $\Theta = 90$ deg. direction are used for comparison. Figure 7 shows the calculated and measured spectra at four jet temperature ratios ranging from 1.0 to 2.72. As can readily be seen, there is again good agreement in each case.

To provide a global comparison of the calculated results of formula (36) and experimental measurements over a broad range of jet velocity and temperature, the peak value of $S(R, \Theta, \phi; \frac{1}{u_j} \frac{D_j}{u_j})$ at $\Theta = 90$ deg. are plotted in figures 8a and 8b as a function of $\frac{u_j}{a_\infty}$. It was found in Ref. [10], the data in such a plot tended to align themselves along nearly parallel lines according to the jet temperature ratio $\frac{T_j}{T_\infty}$. Figure 8a shows the comparison between the calculated results of formula (36) and the data from Ref. [10] and [32]. On considering that there is a fair amount of scattering in the experimental data, the overall agreement is excellent. Here the jet temperature ratio varies over a range of 5. This brackets all present day commercial jet engine operating conditions. The calculated noise level and measurements are in close agreement at nearly every temperature ratio. Figure 8b shows the comparison between the calculated

results and the measurements of Tanna *et al.*³³ and Ahuja³⁴. There is a fair amount of scattering of the subsonic jet data. But they cluster around formula (36). There is also good agreement at supersonic jet velocities. As noted before, the NASA Langley data¹⁰ is consistently 1 to 2 dB higher than the Tanna *et al.*³³ data. The calculated results appear to lie right between these two sets of measurements.

6. Concluding Remarks

In this work a semi-empirical theory for the prediction of the fine scale turbulence noise component of high speed jets is developed. The fine scale turbulence noise is the dominant noise component in the sideline and upstream directions. By comparison with experimental measurements over a wide range of jet velocity and temperature ratios, it is found that the theory can provide very accurate noise prediction.

The present theory is semi-empirical. Two critical components of the theory are the model two-point space-time noise source correlation function and the $k - \epsilon$ turbulence model. Both models contain a fair amount of empiricism. There is, therefore, room for improvements. Theoretically, it would be desirable to be able to derive the two-point space-time correlation function from first principle and/or to replace the $k - \epsilon$ model by a less empirical turbulence theory. But such an endeavor is beyond the scope of the present work.

Despite the inherent semi-empirical nature of the present theory, the accuracy of the prediction over such a broad range of jet velocities and temperatures makes it superior to other methods in the literature and in practice. The present method can provide accurate spectral prediction that is vital to applications in which the use of the perceived noise level (PNdB) is required. The prediction of noise spectrum has proven to be most difficult in the past. Many existing theories are capable of calculating only noise intensity. From a practical standpoint, we believe the present work should be of interest to the aeroacoustics community in need of a better jet noise prediction methodology.

Acknowledgments

This work was supported primarily by NASA Grant NAG3-1683. The authors also wish to acknowledge the support of NASA Grant NAG1-1776 for one of them (CKWT) and NASA Grant NAG3-2102 for the other (LA) during the final phase of this investigation. In addition, the authors wish to thank J.M. Seiner and T.D. Norum of the NASA Langley

Research Center for providing additional data not appearing in their published papers.

References

1. Lighthill, M.J., "On Sound Generated Aerodynamically: I. General Theory", *Proc. Roy. Soc. London Ser. A*, vol. 211, 1952, pp. 564-581.
2. Lighthill, M.J., "On Sound Generated Aerodynamically: II. Turbulence as a Source of Sound", *Proc. Roy. Soc. London Ser. A*, vol. 222, 1954, pp. 1-32.
3. Atvars, J., Schubert, L.K. and Ribner, H.S., "Refraction of Sound from a Point Source Placed in an Air Jet", *J. Acoust. Soc. Amer.*, vol. 37, 1965, pp. 168-170.
4. Lilley, G.M., "On the Noise from Jets", *Noise Mechanisms*, AGARD-CP-131, 1974, pp. 13.1-13.12.
5. Ffowcs-Williams, J.E., "The Noise from Turbulence Convected at High-Speed", *Philos. Trans. Roy. Soc. London Ser. A*, vol. 255, 1963, pp. 469-503.
6. Lilley, G.M., "Jet Noise Classical Theory and Experiments". In *Aeroacoustics of Flight Vehicles: Theory and Practice*, Vol. 1, ed. H.H. Hubbard, pp. 211-289, 1991, NASA RP-1258.
7. Tam, C.K.W., "Jet Noise Generated by Large Scale Coherent Motion". In *Aeroacoustics of Flight Vehicles: Theory and Practice*, Vol. 1, ed. H.H. Hubbard, pp. 311-390, 1991, NASA RP-1258.
8. Tam, C.K.W., "Supersonic Jet Noise", *Annu. Review Fluid Mech.*, vol. 27, 1995, pp. 17-43.
9. Tam, C.K.W., "Jet Noise: Since 1952", *Theor. & Comput. Fluid Dyn.*, to appear 1998.
10. Tam, C.K.W., Golebiowski, M. and Seiner, J.M., "On the Two Components of Turbulent Mixing Noise from Supersonic Jets", *AIAA Paper 96-1716*, 1996.
11. Tam, C.K.W. and Morris, P.J., "The Radiation of Sound by the Instability Waves of a Compressible Plane Turbulent Shear Layer", *J. Fluid Mech.*, vol. 98, 1980, pp. 349-381.
12. Tam, C.K.W. and Burton, D.E., "Sound Generated by Instability Waves of Supersonic Flows. Part 1, Two-Dimensional Mixing Layer; Part 2, Axisymmetric Jets", *J. Fluid Mech.*, vol. 138, 1984, pp. 249-295.
13. Tam, C.K.W. and Chen, P., "Turbulent Mixing Noise from Supersonic Jets", *AIAA J.*, vol. 32, Sept. 1994, pp. 1774-1780.
14. Tam, C.K.W., "Influence of Nozzle Geometry on the Noise of High-Speed Jets", *AIAA Paper 98-2255*, 1998.
15. Khavaran, A., Krejsa, E.A. and Kim, C.M., "Computation of Supersonic Jet Mixing Noise from an Axisymmetric CD Nozzle using $k-\epsilon$ Turbulence Model", *AIAA Paper 92-0500*, Jan. 1992.
16. Khavaran, A., Krejsa, E.A. and Kim, C.M., "Computation of Supersonic Jet Mixing Noise for an Axisymmetric Convergent-Divergent Nozzle", *J. Aircraft*, vol. 31, May 1994, pp. 603-609.
17. Bailly, C., Bechara, W., Lafon, P. and Candel, S., "Jet Noise Predictions using a $k-\epsilon$ Turbulence Model", *AIAA Paper 93-4412*, Oct. 1993.
18. Bailly, C., Lafon, P. and Candel, S., "Computation of Subsonic and Supersonic Jet Mixing Noise using a Modified $k-\epsilon$ Model for Compressible Free Shear Flows", *Acta Acustica*, vol. 2, Apr. 1994, pp.101-112.
19. Bailly, C., Candel, S. and Lafon, P., "Prediction of Supersonic Jet Noise from a Statistical Acoustic Model and a Compressible Turbulence Closure", *J. Sound and Vib.*, vol. 194, 1996, pp. 219-242.
20. Bailly, C., "A Statistical Description of Supersonic Jet Mixing Noise", *AIAA Paper 97-1575*, May 1997.
21. Tennekes, H. and Lumley, J.L. *A First Course in Turbulence*, Chapter 2. The MIT Press, 1978.
22. Feynman, R.P., Leighton, R.B. and Sands, M. *The Feynman Lectures on Physics*, vol 1. Chapter 39, 1963, Addison-Wesley. New York.
23. Liepman, H.W. and Reshko, A. *Elements of Gasdynamics*. Chapter 14, 1957, John Wiley & Sons. New York.
24. Favre, A. "Equations des Gaz Turbulents Compressibles", *J. de Mecanique*, vol. 3, 1965, pp. 361-390.
25. Speziale, C.G., "Turbulence Modeling for Time Dependent RANS and VLES: A Review", *AIAA J.*, vol. 36, Feb. 1998, pp. 173-184.
26. Knight, D.D., "Numerical Simulation of Compressible Turbulent Flows using the Reynolds-Averaged Navier-Stokes Equations", *AGARD Report R-819*, 1997.
27. Tam, C.K.W. and Auriault, L., "Computation of Mean Flow Refraction Effects on Jet Noise", *AIAA Paper 97-1599*, May 1997.
28. Davies, P.O.A.L., Fisher, M.J. and Barratt, M.J., "The Characteristics of the Turbulence in the Mixing Region of a Round Jet", *J. Fluid Mech.*, vol. 15, 1963, pp. 337-367.
29. Chu, W.T., "Turbulence Measurements Relevant to Jet Noise", *Institute for Aerospace Studies, U. of Toronto*, UTIAS Report No. 119, Nov. 1966.
30. Pope, S.B., "An Explanation of the Turbulent Round Jet/Plane-Jet Anomaly", *AIAA J.*, vol. 16, no. 3, 1978, pp. 279-281.
31. Thies, A.T. and Tam, C.K.W., "Computation of Turbulent Axisymmetric and Nonaxisymmetric Jet Flows using the $k-\epsilon$ Model", *AIAA J.*, vol. 34, Feb. 1996, pp. 309-316.
32. Norum, T.D. and Brown, M.C., "Simulated High Speed Flight Effects on Supersonic Jet Noise", *AIAA Paper 93-4388*, Oct, 1993.
33. Tanna, H.K., Dean, P.D. and Burrin, R.H., "The Generation and Radiation of Supersonic Jet Noise, Vol. III, Turbulent Mixing Noise Data", *Technical Report AFAPL-TR-76-65*, Air Force Aero Propulsion Laboratory, WPAB, June 1976.
34. Ahuja, K.K., "Correlation and Prediction of Jet Noise", *J. Sound and Vib.*, vol. 29, 1973, pp. 155-168.
35. Tam, C.K.W., "Broadband Shock Associated Noise of Moderately Imperfectly Expanded Supersonic Jets", *J. Sound and Vib.*, vol. 140, 1988, pp. 55-71.

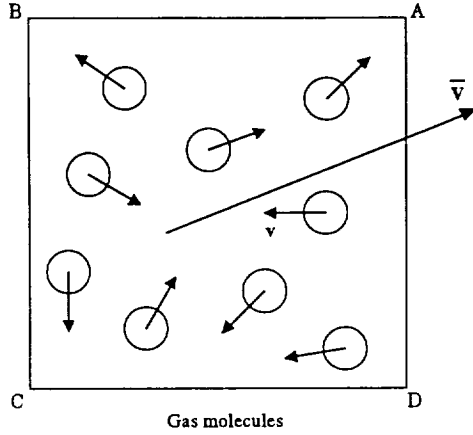


Figure 1. Random motion of gas molecules in the moving frame fixed to the mean velocity \bar{V} .

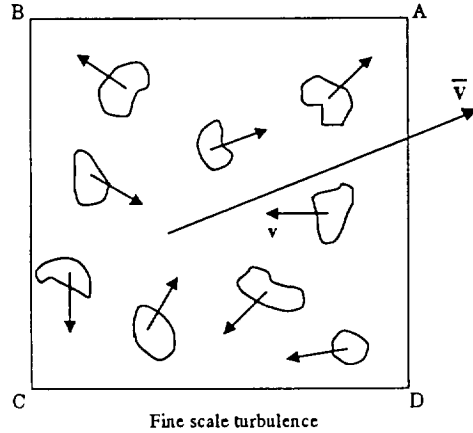


Figure 2. Random motion of blobs of fine scale turbulent fluid in a frame of reference moving with the mean velocity \bar{V} .

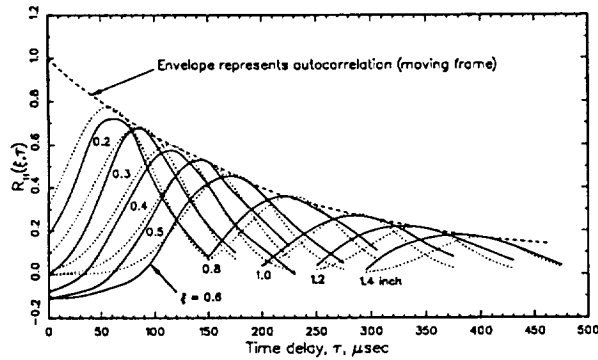


Figure 3. Two-point space-time correlation of the axial velocity component in a jet. — measured data, Davies et al. (1963), model function.

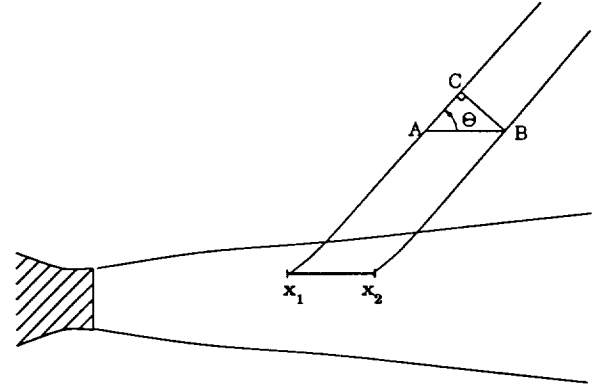


Figure 4. Schematic diagram showing the difference in ray paths between source points x_1 and x_2 from a far field point x with spherical coordinates (R, Θ, ϕ) .

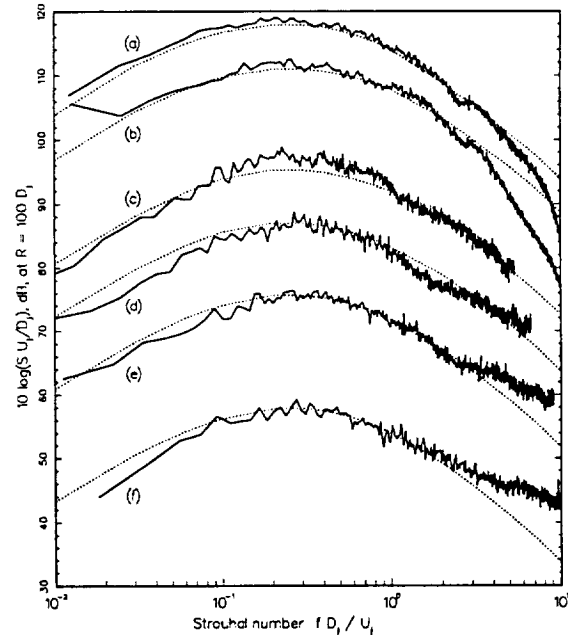


Figure 5a. Cold jet noise spectra at $\Theta = 60$ deg., $T_r/T_\infty = 1.0$.
(a) $M_j = 2.0$, (b) $M_j = 1.49$, (c) $M_j = 0.9$, (d) $M_j = 0.7$,
(e) $M_j = 0.5$, (f) $M_j = 0.3$. — experiments, Ref [10],[32]
..... equation (36).

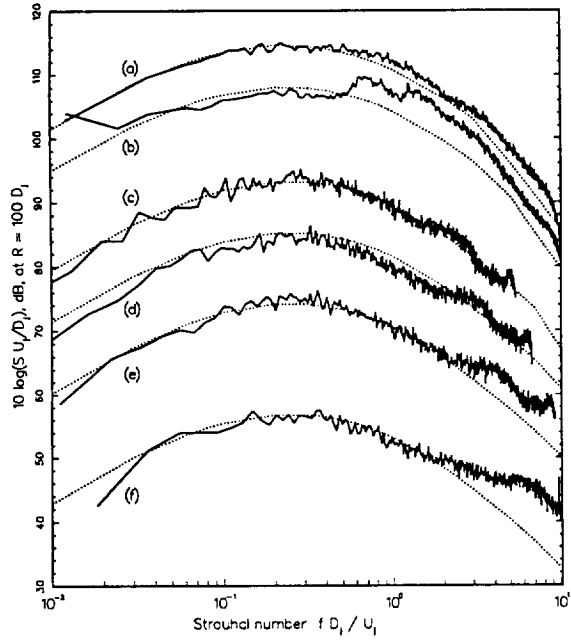


Figure 5b. Cold jet noise spectra at $\Theta = 90$ deg., $\frac{T_r}{T_\infty} = 1.0$.
 — experiments ; equation (36).

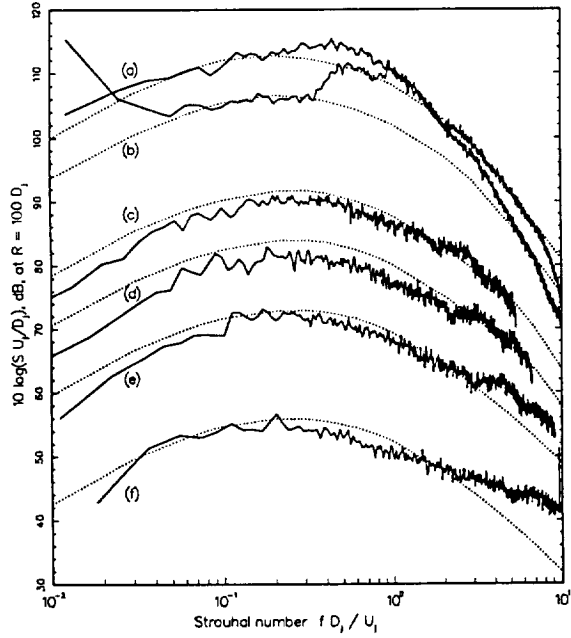


Figure 5c. Cold jet noise spectra at $\Theta = 120$ deg., $\frac{T_r}{T_\infty} = 1.0$.
 — experiments ; equation (36).

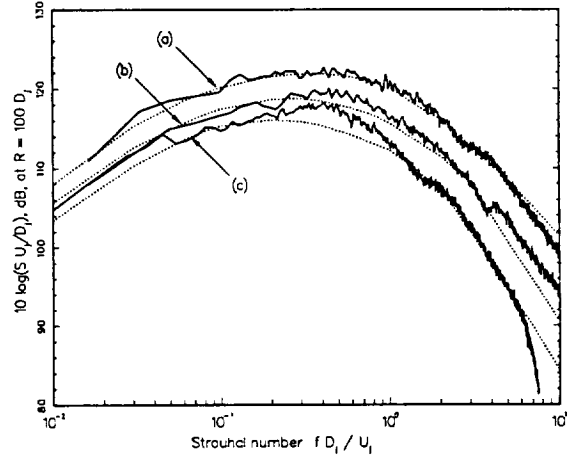


Figure 6. Hot jet noise spectra at $M_j = 2.0$, $\frac{T_r}{T_\infty} = 1.8$.
 (a) $\Theta = 69$ deg., (b) $\Theta = 91$ deg., (c) $\Theta = 117$ deg.
 — experiments, Ref [10] ; equation (36).

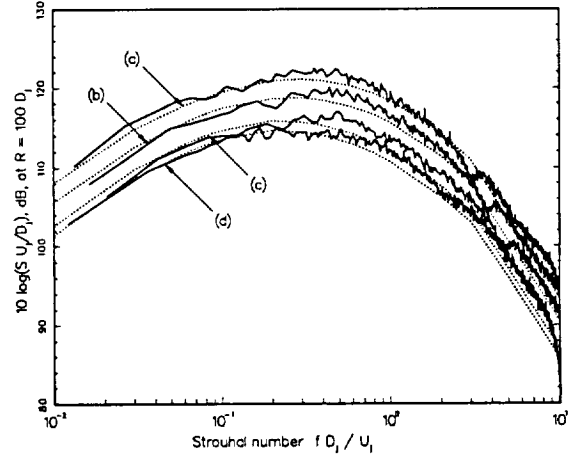


Figure 7. Effect of jet temperature on the noise spectrum at 90 degrees for a Mach 2.0 jet.
 (a) $\frac{T_r}{T_\infty} = 2.72$, (b) $\frac{T_r}{T_\infty} = 1.8$, (c) $\frac{T_r}{T_\infty} = 1.12$, (d) $\frac{T_r}{T_\infty} = 1.0$.
 — experiments ; equation (36).

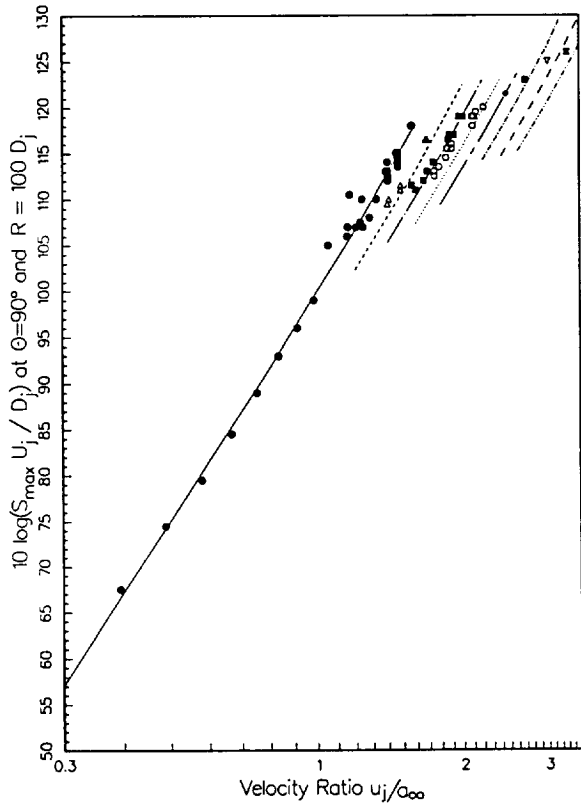


Figure 8a. Dependence of the peak level of the noise spectrum at $\Theta = 90^\circ$ on velocity and temperature ratios.

T_r/T_∞	1.0	1.4	1.8	2.2
measurements	●	△	■	○
equation (36)	—	---	---
T_r/T_∞	2.7	3.3	4.1	4.9
measurements	◆	⊠	▽	⊞
equation (36)	---	---	---
Data from Ref [10] and [32].				

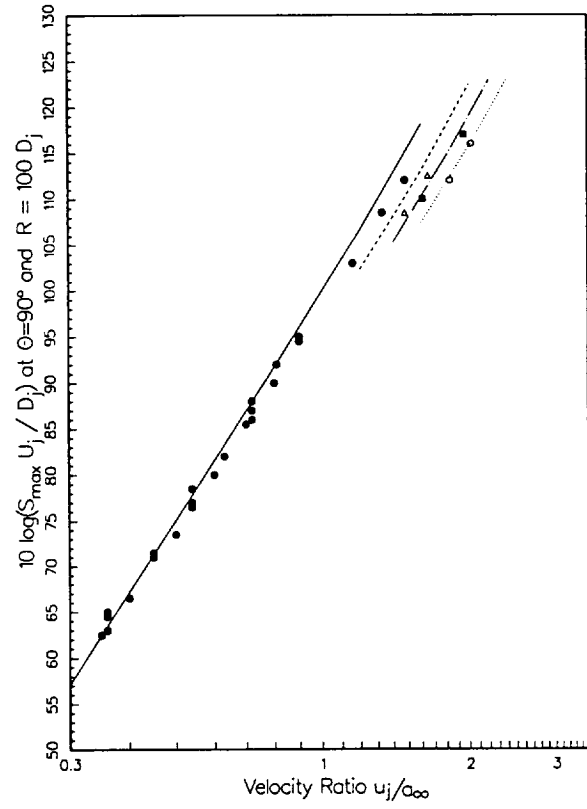


Figure 8b. Same as 8a. Data from Ref [33] and [34].